

The evolution of planetesimal swarms in self-gravitating protoplanetary discs

Joe Walmswell¹*, Cathie Clarke¹ and Peter Cossins²

¹*Institute of Astronomy, Madingley Rd, Cambridge, CB3 0HA, UK*

²*Dept. of Physics and Astronomy, University of Leicester, Leicester, LE1 7RH*

February 2013

ABSTRACT

We investigate the kinematic evolution of planetesimals in self-gravitating discs, combining Smoothed Particle Hydrodynamical (SPH) simulations of the disc gas with a gravitationally coupled population of test particle planetesimals. We find that at radii of 10s of au (which is where we expect planetesimals to be possibly formed in such discs) the planetesimals' eccentricities are rapidly pumped to values > 0.1 within the timescales for which the disc is in the self-gravitating regime. The high resulting velocity dispersion and the lack of planetesimal concentration in the spiral arms means that the collision timescale is very long and that the effect of those collisions that do occur is destructive rather than leading to further planetesimal growth. We also use the SPH simulations to calibrate Monte Carlo dynamical experiments: these can be used to evolve the system over long timescales and can be compared with analytical solutions of the diffusion equation in particle angular momentum space. We find that if planetesimals are only formed in a belt at large radius then there is significant scattering of objects to small radii; nevertheless the majority of planetesimals remain at large radii. If planetesimals indeed form at early evolutionary stages, when the disc is strongly self-gravitating, then the results of this study constrain their spatial and kinematic distribution at the end of the self-gravitating phase.

Key words: accretion discs - gravitation - planetary systems: formation, protoplanetary discs

1 INTRODUCTION

There are commonly discussed mechanisms by which gas giant planets can form out of the gas and dust of the protoplanetary disc. On the one hand, part of the disc may become sufficiently dense to become gravitationally unstable and collapse (Boss 2000). Alternatively, in what has become to be known as the ‘core accretion’ scenario, the dust in the disc coagulates to form ever larger objects, the planetesimals, eventually resulting in a solid core that is large enough to initiate runaway accretion of a gaseous envelope (e.g. Pollack et al. (1996), Hubickyj et al. (2005)). In the latter scenario planetesimal coagulation must occur while the disc is still gas rich (in contrast to the case of the assembly of terrestrial planets, where the process may occur after dispersal of the disc gas). Unsurprisingly, therefore, there is a large literature devoted to planetesimal evolution in the presence of gas (Adachi et al. (1976), Pollack et al. (1996), Tanaka & Ward (2004)). In most cases, the gas is treated as a laminar flow although several authors

(Laughlin et al. (2004), Nelson & Papaloizou (2004), Nelson (2005), Ida et al. (2008), Nelson & Gressel (2010)) have considered instead the scenario where planetesimals are subject to stochastic torques arising from fluctuations in a disc subject to turbulence generated by the magneto-rotational instability (MRI). In the case of laminar discs, planetesimal eccentricity is (weakly) pumped by mutual gravitational scattering (e.g. Safronov (1969)) and (weakly) damped by gas drag, so that the equilibrium distribution of eccentricities is peaked at low values (~ 0.01). This low value is important to continued planetesimal growth since it implies low relative velocities for planetesimal encounters: this not only favours agglomerative (as opposed to destructive) outcomes (Benz & Asphaug (1999), Leinhardt et al. (2008)) but also enhances the collision cross-section ($\propto e^{-2}$) in the gravitationally-focused regime.

All of the above studies treat the evolution of planetesimals in *non*-self-gravitating discs. However, Rice et al. (2004) have argued that planetesimals may be formed very early (in the first few 10^5 years) of a disc's life when it is still strongly self-gravitating; at this stage, spiral features in the disc provide pressure maxima in which dust is concen-

* E-mail: jjw49@ast.cam.ac.uk

trated through the action of gas drag. The enhanced collision rates are favourable to grain growth and Rice et al. (2006) have argued that self-gravity in the *dust* phase may even promote the formation of km scale structures (i.e. planetesimals). Observational evidence for at least the early stages of grain growth during the self-gravitating phase is provided by the detection of 10 cm radiation from HL Tau (Greaves et al. 2008), which implies that the growth of grains to at least cm scales (from the sub-micron scales typifying the interstellar medium) has already occurred in this young and massive disc system.

If planetesimal formation indeed belongs to the earliest (self-gravitating) phase of disc evolution, then it is necessary also to trace the evolution of planetesimals during the self-gravitating phase. The dynamical evolution of planetesimals in this environment has a number of implications for planet formation and for the collisional production of dust in disc systems. For example, the relative importance of collisional growth of planetesimals in the self-gravitating and non-self gravitating phase of the disc can be crudely assessed (cf Britsch et al. (2008)) by comparing the product of the lifetime of each phase, the typical disc density and the (inverse) square of the typical planetesimal velocity dispersion. The first two terms roughly cancel (i.e discs typically live an order of magnitude longer in the non-self gravitating phase but with disc masses an order of magnitude lower) so the relative importance of collisional growth in the two regimes boils down to the relative values of the velocity dispersion.

A pilot study of the dynamical evolution of planetesimals in self-gravitating discs (Britsch et al. 2008) demonstrated that high orbital eccentricities (e) are generated in such discs with particles undergoing stochastic changes in their orbital elements as a result of interaction with spiral features in the disc: high eccentricities imply a high velocity dispersion (of order ev_k where v_k is the local Keplerian velocity) if the particle trajectories are randomly phased. A lower velocity dispersion would however apply if the planetesimals instead demonstrated local velocity coherence: the small number of particles modeled by Britsch et al. (2008) did not permit exploration of this possibility however. For the same reason, it was not possible to discern the sign of any net migration of the planetesimal swarm nor whether the main statistical effect involved changes in orbital energy or angular momentum. All these issues have implications for planetesimal growth during the self-gravitating phase and also for the retention of planetesimals against loss through radial migration (Takeuchi et al. 2005) or collisional grinding to small dust (Wyatt et al. 2007). Moreover, evolution during the self-gravitating phase controls the spatial distribution and dynamical properties of any planetesimals that survive this phase.

All of the above provides ample motivation for the present study in which we explore the response of a large ensemble of planetesimals to the gravitational torques imposed by a self-gravitating gas disc. We restrict ourselves to the regime where planetesimals respond as test particles to the imposed potential fluctuations. This in practice restricts us to sizes $>$ km scale (in order to be able to neglect gas drag; Britsch et al. (2008)) and $<$ 1000 km scale (in order to be in the test particle regime where the effect of gravitational perturbations induced by the particles in the disc gas can be ignored; Bate et al. (2003)).

In Section 2 we present a numerical investigation (modeling the disc with Smoothed Particle Hydrodynamics (SPH)) that extends the pilot study of Britsch et al. (2008) to a large ensemble of planetesimals. Our results (Section 3) imply the disc pumps particle eccentricity with only modest changes in the semi-major axis and this motivates the analytical modeling and Monte Carlo simulations that we present in Section 4. This analytical/Monte Carlo approach is able to reproduce the results of the SPH simulation over the rather limited time frame that is possible in the latter case and also permits integration over long timescales. In Section 5 we discuss the results of these calculations in relation to the questions posed above and summarise our conclusions.

2 THE SIMULATION

2.1 The physics of self-gravitating discs

We model the gas disc as a self-gravitating disc which achieves a situation of *self-regulation*: i.e. it settles to a marginally-stable state where the Toomre Q parameter (Toomre 1964) obeys

$$Q = \frac{c_s \kappa}{\pi G \Sigma} \sim 1. \quad (1)$$

Here c_s is the local sound speed, Σ the gas surface density and κ is the epicyclic frequency, which is $\sim \Omega$ (the Keplerian frequency) for the low mass discs considered here. In this state the disc is in a state of thermal equilibrium between the heating associated with the gravitational instability and the imposed cooling. Here we follow Gammie (2001) and Lodato & Rice (2005) in parameterising the cooling in terms of a cooling time that is a fixed multiple (β) of the local dynamical time (Ω^{-1}), i.e. we have $t_{\text{cool}} = \beta \Omega^{-1}$ and

$$Q_- = -\frac{u}{t_{\text{cool}}} \quad (2)$$

where Q_- and u are the cooling rate per unit mass and thermal energy per unit mass.

The parameter β is a measure of overall cooling and the choice of β determines the magnitude of the spiral density waves required to maintain thermal equilibrium. By equating this cooling law with the predicted heating rate per unit mass Q_+ from the instability, Cossins et al. (2009) demonstrated that the fractional density perturbation, a measure of relative spiral arm strength, is proportional to $\beta^{-1/2}$; the numerical simulations in the same study confirmed this dependency and suggested that

$$\frac{\delta \Sigma}{\Sigma} \approx \frac{1}{\sqrt{\beta}}. \quad (3)$$

This means that in our constant β simulations we would expect the density perturbation to be approximately constant across the disc and to increase as β decreases. In practice, if β is less than about 4 in a simulation, the magnitude of the perturbation becomes non-linear and the disc fragments (Gammie 2001). (See e.g. Meru & Bate (2011), Meru & Bate (2012), Lodato & Clarke (2011), Paardekooper et al. (2011), Paardekooper (2012) and Rice et al. (2012)) for an ongoing debate as to whether fragmentation may also eventually occur in well resolved simulations at significantly higher values of β .)

2.2 Simulation parameters

We model the system as a point mass, mass M , orbited by 250,000 SPH gas particles and 50,000 test particles; for details of the code see Cossins et al. (2009) and references therein. The test particles are assigned masses equal to 10^{-6} times the mass of a gas particle and are subject only to gravitational forces. Gas particles are accreted onto the point mass if they enter within a sink radius of 0.25 code units and satisfy certain conditions (Bate et al. 1995); the point mass itself is free to move. By the end of the simulation, no more than 2 per cent of the gas particles are accreted.

Artificial viscosity is included, according to the standard SPH formalism, with $\alpha_{\text{SPH}} = 0.1$ and $\beta_{\text{SPH}} = 0.2$; for the parameters employed, the ratio of SPH smoothing length to disc vertical scale height is about two throughout. The gas is modelled as a perfect gas with $\gamma = 5/3$ and is subject to both compressive heating and shock dissipation. The cooling law (Equation 2) means that heat loss depends only on the dimensionless parameter β , so cooling is scale free. For the main simulation we adopt $\beta = 5$ which corresponds to rather large amplitude spiral perturbations (see Equation 3); we contrast these results with the lower amplitude case where $\beta = 10$.

We employ scaled units so that $G = M = 1$ and express time in units of the dynamical time $t_{\text{dyn}} = \Omega^{-1}$ at $R=1$. This time t always refers to the time since the start of the simulation. We use these dimensionless results because they can be easily scaled to real situations. Our standard model consists of a disc with total mass equal to 0.1, distributed with surface density $\propto R^{-3/2}$ over the radial range 1 to 25 and the planetesimals are distributed according to the same radial distribution; we also investigate a similar set-up but with $\beta = 10$ and total mass of 0.5. We initialise the simulations with uniform temperature so that $Q = 2$ at all radii in the disc. At each radius we distribute the particles in z in a Gaussian distribution representing approximate hydrostatic equilibrium at the initial temperature. True hydrostatic equilibrium is reached within a few local dynamical times.

3 SIMULATION RESULTS

The disc is initialised with $Q = 2$ throughout and is thus initially gravitationally stable. It then cools on the local cooling time until it attains $Q = 1$, initiating the gravitational instability and liberating heat. By time $t = 4000$ the disc has definitely settled into a quasis-steady state where spiral features form and dissolve on a roughly dynamical timescale and with $Q = 1$ for $5 < R < 25$. (At $R < 5$ the value of Q rises above unity since the disc is poorly resolved and heating by artificial viscosity acting on the Keplerian velocity field is sufficient to maintain the disc in a gravitationally stable state.) Since this is a purely numerical artefact, we restrict our attention to the regime $R > 5$.

3.1 Escapees

The first consideration is whether the test particles of the swarm gained enough energy from their interactions with the disc to escape the system entirely. We assess this by

calculating the energies of the test particles (for this purpose we approximate the potential due to the disc by simply - for each particle - adding the enclosed disc mass to the effective mass of the central object and ignoring the contribution from external particles; although this is not strictly correct in a disc system, this does not significantly impair our ability to differentiate between bound and unbound particles).

We find that (once the disc has settled into a steady gravoturbulent state) around 200 particles (out of a total of 10^5) escape during the subsequent 4000 time units. If we (somewhat arbitrarily) equate code units for mass and radius with $1M_{\odot}$ and 1 au then this implies an e-folding timescale of 3×10^5 years (i.e. of order the self-gravitating lifetime of the disc). This e-folding timescale is likely to be an under-estimate for two reasons: the low value of β employed in the simulations (which implies much more vigorous spiral activity than would be expected given the relatively long cooling timescales in realistic protostellar discs; Clarke (2009) and Stamatellos et al. (2007)) and the assumption of constant disc mass (whereas in reality the disc mass would decline over such timescales).¹ On this basis, we conclude that the majority of planetesimals would in reality remain bound.

3.2 Ring spreading

Once the system has settled into the equilibrium state (i.e. after $t = 3 - 4000$) we identify rings of particles over a restricted radial range and analyse their spatial evolution. Figure 1 illustrates the rather rapid spreading after five local orbital periods of a ring of initial width 1, initially located at $R = 10$ at $t = 4000$. We find that the fractional change in the centroid of the distribution and the change in the width of the distribution (normalised to the initial radius) is independent of the radius of the ring selected as long as the comparisons are conducted after the same number of local dynamical timescales. This is as expected, given that (for the constant β that we impose) the fractional amplitude of the gravitational perturbations should be independent of radius. Note that although the mode of the particle radii has moved in slightly, the mean has moved out. Figure 2 illustrates the evolution of the fractional standard deviation of a ring at $R = 20$ selected at $t = 3500$ and illustrates the continued spreading of the ring over many local orbital times.

We find that the rings spread in response to stochastic interaction with the disc and also that there is a small outward shift in the particle centroid for each ring. We can understand this behaviour by considering the evolution of the energy distribution of particles in a selected ring (Figure 3): the finite width of the initial distribution just reflects the finite width of the ring. It is notable that there is little evolution in the distribution of particle energies over the time period of $t = 4000$ to $t = 7500$, whereas ring spreading is still significant over this period (Figure 2). Although this

¹ We found an approximately 3 times higher escape rate in the case of our massive disc simulation (with disc mass five times higher than the standard case), which demonstrates that - as expected - the rate of test particle escape would drop as the disc mass declines.

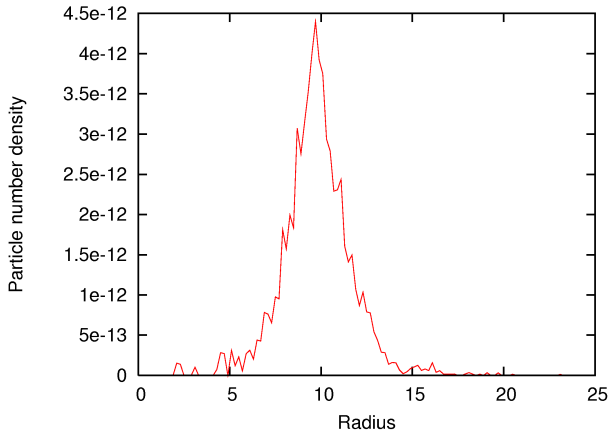


Figure 1. Ring profile for $R = 10$ after five local periods and with initial width of 1 at time $t = 4000$.

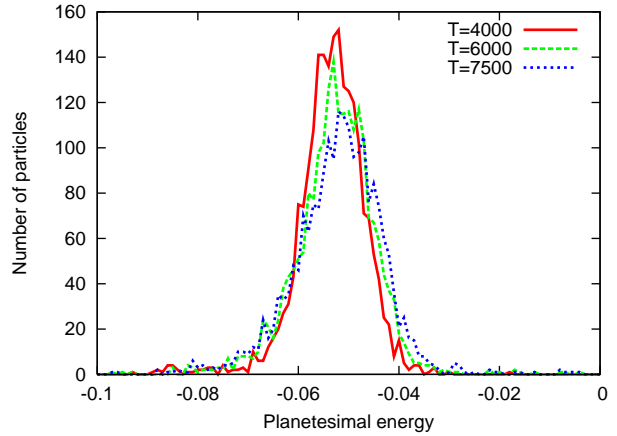


Figure 3. Evolution of the energy distribution of the $R=10$ ring, selected at $t=4000$.

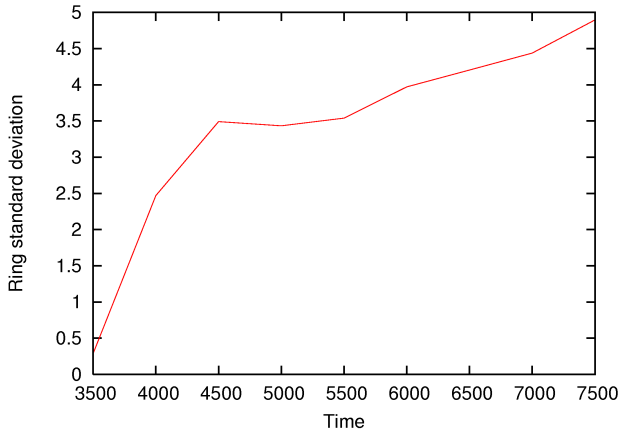


Figure 2. Evolution of the ring standard deviation at $R = 20$. The ring is selected at $t = 3500$, when the disc is in the quasi-steady state, and then followed for the rest of the simulation.

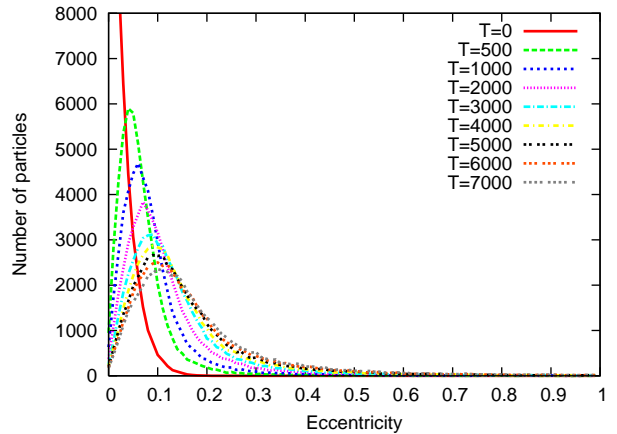


Figure 4. Eccentricity evolution of the standard simulation.

spreading can be partially attributed to phase mixing (given the finite eccentricities of the particles selected), this is not the only process at work, as is illustrated by Figure 5, which shows the secular increase of the particle eccentricities. This suggests that as an ensemble, the particles are undergoing little evolution in energy but are diffusing in angular momentum. This implies a growth of particle eccentricity which we quantify below for the entire disc. (It should be stressed that the constancy of energy - and hence semi-major axis - is a property of the local ensemble; as was noted in Britsch et al. (2008), individual particles undergo stochastic interactions in which they undergo modest changes in energy).

3.3 Eccentricity growth

Figure 4 depicts the eccentricity distribution for the entire disc ensemble over the duration of the simulation and confirms the evolution towards higher eccentricity, as would be expected if the spatial spreading largely reflects the growth of particle eccentricity at fixed semi-major axis. Note that in the period before the disc reaches the quasi-steady state (i.e. between $t = 0$ and $t = 3 - 4000$) the eccentricity distri-

bution is not being pumped by the recurrent spiral features. There does not appear to be a sharp transition between the two regimes though.

In Figure 5 we compare the evolution of the mean eccentricity between the standard simulations and the high β case (in which β differs by a factor of 2). We see that the timescale to attain a given mean eccentricity is roughly doubled in the higher β case. This is consistent with a picture in which the particles are responding diffusively to gravitational interactions with the disc: the diffusion timescale scales with the inverse of the diffusion coefficient and thus with the inverse square of the amplitude of the perturbations. Hence (from Equation 3) we expect the timescale for eccentricity growth to scale linearly with β , as is consistent with Figure 5. We note that the mean eccentricity increases smoothly after $t = 500$ and that, as with the distribution as a whole, we cannot identify a sharp transition when the quasi-steady state is reached. This means that we can consider the distribution to be a reasonable proxy for how it would appear had the disc been in the quasi-steady state throughout, a fact we use in Section 4 to scale our analytical model and Monte Carlo simulations.

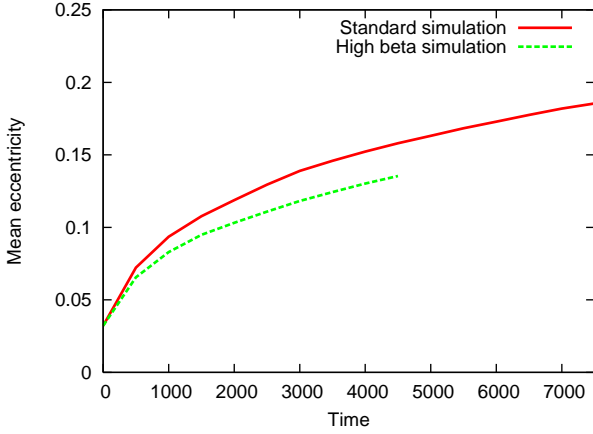


Figure 5. Evolution of the eccentricity means for the two simulations.

3.4 The velocity dispersion

For a swarm of particles with randomly orientated orbits, the velocity dispersion is approximately equal to the product of the eccentricity and the local Keplerian velocity (Britsch et al. 2008). The strong growth in particle eccentricity would thus raise the velocity dispersion of the planetesimals with consequences for particle growth that we discuss below. However, this would be an over-estimate of the velocity dispersion if there was a degree of local velocity coherence within the particle swarm. We investigate this in Figure 6 by comparing the evolution of the local velocity component (σ) and its three orthogonal components (computed within a patch of disc containing ~ 100 particles) with the product of the instantaneous mean eccentricity and the local Keplerian velocity ($\sigma_p = ev_k$). The figure illustrates that ev_k is indeed a good measure of the local velocity dispersion, as is expected in the case of randomly phased elliptical orbits. In addition, the ratio between the radial and azimuthal dispersions is maintained at about 3:2. One can show from the epicyclic approximation for a cylindrical potential that the expected ratio between the dispersions should be $\sigma_\phi^2 = 0.5\sigma_R^2$ (Binney & Tremaine 2008), i.e. that $\sigma_\phi = \sigma_R/\sqrt{2}$ or $3\sigma_\phi \approx 2\sigma_R$.

The growth of the velocity dispersion has profound consequences. First, a high velocity dispersion suppresses the role of gravitational focusing in facilitating collisions (Britsch et al. 2008). In the limit that the disc scale height exceeds the mean separation between planetesimals the timescale for physical collisions between planetesimals of mass M , radius R and density ρ is

$$t_{\text{grow}} \sim \frac{\rho^{2/3} M^{1/3}}{\Sigma_p \Omega (1 + 4GM/(R\sigma^2))}, \quad (4)$$

where Σ_p is the planetesimal surface density and σ is the planetesimal velocity dispersion. The σ dependence means that collisions are highly disfavoured. At 30 au from a solar mass star and using $e = 0.2$, the velocity dispersion is around 1 km s^{-1} . Using the above formula for 100 km planetesimals, the collision timescale is of order 10^9 years! Smaller planetesimals would give even longer timescales. Since planetesimal growth cannot proceed without physical collisions,

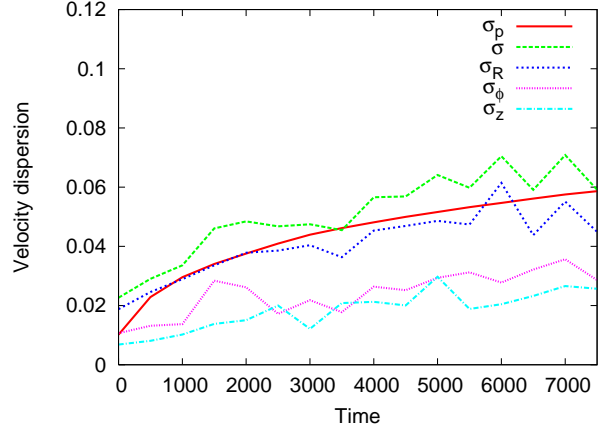


Figure 6. Evolution of the velocity dispersion (σ) and its components in the radial (σ_R), azimuthal (σ_ϕ), and vertical (σ_z) directions, compared with the prediction for randomly orientated orbits (σ_p).

this rules out significant planetesimal growth during the self-gravitating phase.

In addition - even when collisions do occur - the collisional velocity is correspondingly high. The velocity required to shatter planetesimals by collision is a few 100 m s^{-1} (Leinhardt et al. 2008), meaning that collisions would tend to result in disruption rather than in growth. We can then use the above collision probabilities to estimate a rough upper limit on the amount of small dust (i.e. in the observable regime of $< 1\text{mm}$) that could be generated by disruptive collisions between planetesimals. On the optimistic assumption that every planetesimal-planetesimal collision results in all its mass being liberated as dust, the fraction of mass in planetesimals that can be liberated is simply the ratio of the self-gravitating lifetime to the collision time, i.e. $\sim 10^{-4}$. We therefore conclude that the role of planetesimal collisions in re-supplying small dust is insignificant during the self-gravitating phase. Once the disc enters the non-self gravitating phase, and gas drag reduces the equilibrium eccentricity level to around 0.01 (Kokubo & Ida 2000), the collision rate rises by around a factor of 100 and at this stage either collisional growth and/or dust production may become important.

3.5 Planetesimal concentration in the arms

The above estimates for planetesimal collision frequencies neglect any possible concentration of particles in spiral features. For the values of β employed in the simulations, the gas surface density varies by no more than a factor of two between the arms and the inter-arm regions (as expected, since we have modeled a regime where the disc is close to - but not at - the fragmentation boundary). If the planetesimals simply followed the gas, such an enhancement would have only a minor effect on planetesimal collision probabilities, even in the unlikely event that planetesimals spent all their time in long-lived regions of density enhancement. In fact we find that - instead of being preferentially concentrated in the arms - the planetesimal surface density varies by no more than $\sim 20\%$ around the orbit in the standard

simulation, i.e. with amplitude much less than that of the gas.²

Britsch et al. (2008) suggested that there were possible hints that the concentration of particles in the arms was more efficient in the case of more massive discs. In their simulation with a disc mass of half that of the point mass they identified epochs at which some test particles would settle into orbits that co-rotated with the spiral modes and conserved a Jacobi constant. We have analysed our ‘massive disc’ simulation and however find that, as in the standard simulation, there is no discernible influence on the planetesimal distribution: there is no significant concentration of planetesimals in the arms.

3.6 A truncated planetesimal distribution

We finally consider the case that the planetesimal distribution is truncated, i.e. that it does not initially extend within a certain inner radius, R_{in} , and study the extent to which planetesimals are scattered into regions within R_{in} . This choice is motivated by the suggestion of Clarke & Lodato (2009) that planetesimals are only likely to form in self-gravitating discs at large radius (beyond a few 10s of au). We also note that the simulations of Gibbons et al. (2012) suggest that the mechanism is probably restricted to radii greater than 20 au. At such radii the cooling time is relatively short (corresponding to $\beta < 10$; Clarke (2009)) and the amplitude of spiral disturbances is large enough for rapid concentration of dust in spiral structures (i.e. on timescales shorter than the (roughly dynamical) lifetimes of spiral features).

We do not need to conduct new simulations for this scenario but - since the planetesimals are non-interacting - simply tag planetesimals that are located at radius $R > 10$ at $t = 5000$ and follow the evolution of their density distribution. From Figure 7, one can see that the distribution rapidly relaxes, with about 10 per cent of the particles moving inward by a time of $t=5500$, although with no discernible further evolution over the time-frame of $t = 5500$ to 7500. The initial relaxation is consistent with the fact that the typical particle eccentricity is already ~ 0.1 at $t = 5000$ and so just represents the fact that particles near the ‘edge’ visit the inner region even without further orbital evolution. We revisit the issue of planetesimal diffusion into an inner cleared region when we construct our analytic model in Section 4.

4 A SIMPLE SCATTERING MODEL

The simulation results encourage the exploration of a scenario in which the evolution of the planetesimal swarm is primarily driven by changes in angular momentum rather than energy. This prompted us to attempt to reproduce our results by modelling the evolution of the swarm as a process

² Note that the initial process of concentrating solid material into spiral features described by Rice et al. (2004) - which is required for the formation of planetesimals in the self-gravitating phase - instead involves the effect of gas drag on small particles, and this, by definition, is ineffective in the test particle regime considered here.

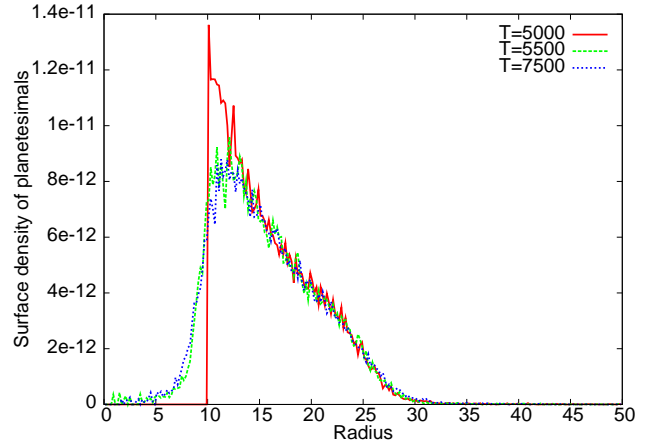


Figure 7. Evolution of the planetesimals initially beyond $R=10$ at time $t=5000$.

of diffusion in angular momentum space. We start by obtaining analytic expressions for the diffusion coefficients, set up the resulting diffusion equation and use Green’s functions to solve for the evolution of the angular momentum distribution (and the associated eccentricity and radial distributions) starting from an arbitrary radial profile and initially circular orbits. The resulting solutions however involve the computation of large numbers of Legendre polynomials and are not of practical use until the system has evolved well away from the initial delta function distribution of eccentricities. We nevertheless obtain solutions for the eccentricity distribution that are a reasonable representation of the SPH results at the end of the simulation. We can also compute the subsequent evolution of the system and derive expressions for the final (equilibrium) distributions over radius and eccentricity (which correspond to a uniform distribution in angular momentum at every energy). In the following sub-section we then verify these predictions using a simple Monte Carlo model; this approach has the additional advantage that it can be readily generalised to treat the case where the perturbation amplitude is a function of radius.

4.1 Analytic solution

We consider an ensemble of particles orbiting a mass M with fixed semi-major axis a . At some random time in each particle’s orbit the velocity vector is rotated by some angle $\Delta\theta$ in the orbital plane, where θ is the angle between the velocity and radial vectors. This preserves the particle energy but perturbs the angular momentum.

We start by writing the angular momentum per unit mass, L , for a particle at radius r as

$$L^2 = 2GM \sin^2 \theta \left(r - \frac{r^2}{2a} \right). \quad (5)$$

The equation is simplified by letting $x = 1 - r/a$, so that

$$L^2 = GMa(1 - x^2) \sin^2 \theta = L_{\text{max}}^2 \sin^2 \theta, \quad (6)$$

and

$$\frac{dL}{d\theta} = \sqrt{L_{\text{max}}^2 - L^2}. \quad (7)$$

L_{\max} is the maximum local angular momentum and is a function of x (i.e. for particles at given r/a and energy - hence speed - this maximum occurs when the velocity is purely tangential). The angular momentum diffusivity, D , is given by $\Delta L^2/\tau$ where ΔL is the change in angular momentum associated with deflection $\Delta\theta$ and τ is the time between such deflections: for now we assume both $\Delta\theta$ and τ to be constant around the orbit. We will also consider the case where $\Delta\theta$ is independent of a and where τ scales with the orbital period ($\propto a^{3/2}$). This is motivated by the wish to compare with the SPH simulations which are conducted with constant cooling time to dynamical timescale ratio and in which, therefore, the fractional amplitude of gravitational disturbances is independent of radius (see equation (3)).

We can relate ΔL to $\Delta\theta$ via Equation 7 so that the value of D at given x is proportional to $\frac{dL}{d\theta}^2$, that is to say

$$D \propto \left(\frac{dL}{d\theta}\right)^2 \propto GMa(1-x^2) - L^2. \quad (8)$$

The expectation value of D over an entire orbit (at fixed L and a) is obtained by averaging this quantity over time, using the relationship between time interval and r for an elliptical orbit. Thus

$$\frac{dr}{dt} = \frac{\sqrt{GMa}}{r} \sqrt{e^2 - (1-r/a)^2}, \quad (9)$$

where e is the orbital eccentricity, which is related to L and a by

$$L^2 = GMa(1-e^2). \quad (10)$$

Equation 9 is derived from the orbital equation in the appendix. As before, the equation is simplified by substituting x for r , so that

$$dt \propto \frac{a^{3/2}(1-x)}{\sqrt{(e^2-x^2)}} dx. \quad (11)$$

Thus we have that (for fixed a)

$$\langle D \rangle \propto \int_{-e}^{+e} \frac{(GMa(1-x^2) - L^2)(1-x)}{\sqrt{(e^2-x^2)}} dx, \quad (12)$$

where the odd terms integrate to zero over symmetric limits and may be discarded. The remaining even terms are standard integrals (requiring the substitution $x = e \sin w$) and yield

$$\langle D \rangle \propto \frac{1}{2}(GMa - L^2). \quad (13)$$

One can substitute this into Fick's Laws of diffusion to get the following 1D diffusion equation for the angular momentum distribution $h(L, t)$. J is the flux and $A(a)$ is a constant that is determined by the strength of the perturbation and which in general depends on a (see below). In the case that we are currently considering (where the fractional amplitude of perturbations in the disc is independent of radius and where their characteristic timescale τ scales with the orbital period i.e. $\propto a^{3/2}$) then A is proportional to $a^{-3/2}$; under these circumstances the timescale for angular momentum diffusion scales with the local orbital period.

Thus we have

$$J = -\langle D \rangle \frac{\partial h}{\partial L}, \quad (14)$$

$$\frac{\partial h}{\partial t} = -\frac{\partial J}{\partial L}, \quad (15)$$

$$\langle D \rangle = A(a)(GMa - L^2). \quad (16)$$

The form of $\langle D \rangle$ contrasts with other parametrisations in the literature where it increases with L . Adams & Bloch (2009) consider, for example, the case where it is proportional to L . The form of Equation 16 reflects the fact that where perturbations change only the direction of the velocity, the associated angular momentum change goes to zero in the limit of tangential orbits; this form thus prevents diffusion of angular momentum beyond the physical limit set by a circular orbit.

The diffusion equation is then

$$\frac{\partial h}{\partial t} = \frac{\partial}{\partial L} \left(A(a)(GMa - L^2) \frac{\partial h}{\partial L} \right), \quad (17)$$

for which we assume a separable solution: $h(L, t) = M(L)T(t)$ to get

$$\frac{1}{T} \frac{dT}{dt} = \frac{1}{M} \frac{d}{dL} \left(A(a)(GMa - L^2) \frac{dM}{dL} \right) = -k. \quad (18)$$

This gives $T(t) \propto \exp(-kt)$. If k is non-negative there will be no growing solutions. The equation for $M(L)$ is

$$\frac{d}{dL} \left((GMa - L^2) \frac{dM}{dL} \right) + \frac{k}{A(a)} M = 0. \quad (19)$$

Making the substitutions $y = L/(\sqrt{GMa})$ and $k/A(a) = n(n+1)$ converts Equation 19 into the Legendre equation:

$$\frac{d}{dy} \left((1-y^2) \frac{dM}{dy} \right) + n(n+1)M = 0. \quad (20)$$

The solutions must be regular at $y = \pm 1$, so we may use the Legendre polynomials. If this is combined with the solution for t we have

$$h_n(L, t) = c_n \exp(-n(n+1)A(a)t) P_n(L/\sqrt{GMa}). \quad (21)$$

The general solution is a linear combination of the h_n solutions, with the coefficients determined by the initial distribution:

$$h(L, t) = \sum_{n=0}^{\infty} c_n \exp(-n(n+1)A(a)t) P_n(L/\sqrt{GMa}). \quad (22)$$

If the initial distribution consists of N particles in prograde circular orbits, we have $h(L, t=0) = N\delta(L - \sqrt{GMa})$. If we use the orthogonality property of the Legendre polynomials and the fact that $P_n(1) = 1$ for all n , we have

$$h(L, t) = \frac{N}{\sqrt{GMa}} \sum_{n=0}^{\infty} \frac{2n+1}{2} \exp(-n(n+1)At) P_n(L/\sqrt{GMa}). \quad (23)$$

The eccentricity distribution is then obtained by using $f(e)de = h(L)dL + h(-L)dL$. This is because an eccentricity of e may be owing to a prograde or retrograde orbit with angular momenta of the same magnitude. The quantity dL is double-valued for the same reason. Thus from Equation 10 we have:

$$L = \pm \sqrt{GMa(1-e^2)}, \quad (24)$$

and

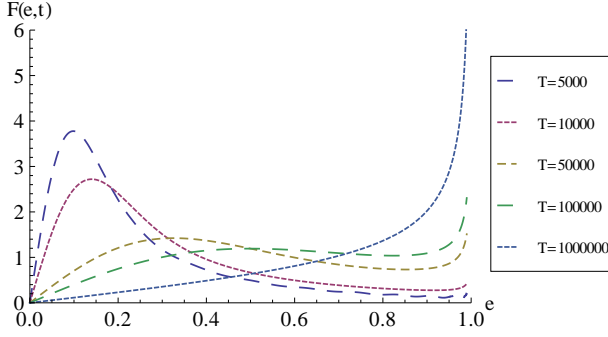


Figure 8. Evolution of the normalised eccentricity distribution.

$$dL = \frac{\mp e \sqrt{GMa}}{\sqrt{1-e^2}} de. \quad (25)$$

The Green's function solution, $f(e, t, a)$ for initially circular orbits at a particular semi-major axis a is therefore

$$f(e, t, a) = \frac{Ne}{\sqrt{1-e^2}} \sum_{n=0}^{\infty} (2n+1) \exp(-n(n+1)A(a)t) P_n(\sqrt{1-e^2}). \quad (26)$$

To consider the behaviour of an entire disc of particles we then calculate an appropriate superposition of Green's functions, bearing in mind (as argued above) that $A = A_0 a^{-3/2}$. For comparison with the SPH simulations, we take a number distribution per unit a that is proportional to $a^{-1/2}$ (since this corresponds to the initial surface density distribution scaling as $R^{-3/2}$) and adopt inner and outer radii of $a_1 = 1$ and $a_2 = 25$. The integrations are straightforward but laborious, making Mathematica the obvious choice. We plot $F(e, t)$ (the distribution function for particle eccentricity) in Figure 8 and have normalised the time unit so as to match the peak in the distribution obtained from the SPH simulation at a time $t=5000$. At $t=0$, $F(e, t)$ is a delta function at $e=0$ but this and the subsequent evolution before $t=5000$ required too many Legendre polynomials to be computationally practicable. We however note the similar form of the curve at $t=5000$ to that obtained in the SPH simulation at the same time (Figure 7). The final distribution occurs when t is large enough such that all the non-constant Legendre terms are effectively zero, leaving $F(e, t) \propto e/\sqrt{1-e^2}$. This is an equilibrium state and represents a uniform angular momentum distribution for particles with the same semi-major axis.

The surface density distribution can be obtained through similar means. Equation 11 gives the probability of a particle with eccentricity e being at x . Multiplying this by $f(e, t, a)$ and integrating with respect to e gives $n(x, t, a)$, the fraction of particles at given semi-major axis in a given interval of x . The lower limit is the value of e for an orbit that achieves the required x value at either periapsis or apoapsis.

$$n(x, t, a) \propto \int_{\max(x, -x)}^1 f(e, t) \frac{1-x}{\sqrt{e^2-x^2}} de. \quad (27)$$

This must be converted to a function of r and a and then normalised so that it represents the distribution resulting from a fixed number of particles. It can then be integrated with the power law distribution for a to get the overall number density.

$$N(r, t) \propto \int_{a_1}^{a_2} n(r, t, a) a^{-1/2} da. \quad (28)$$

$$\Sigma(r, t) = \frac{N(r, t)}{2\pi r}. \quad (29)$$

Again, the integrations are complicated for very many Legendre polynomials. However the solution for the equilibrium distribution is readily obtained. We note that (for a particle swarm of fixed a), the time spent in the interval r to $r+dr$ is $(\frac{dr}{dt})^{-1} dr$, which (using Equation 9 and Equation 5) can be written (for particles of angular momentum L) as

$$dt \propto \frac{r dr}{\sqrt{L_{\max}^2 - L^2}}. \quad (30)$$

Integrating over all values of L from $-L_{\max}$ to L_{\max} we obtain (in general):

$$dt \propto r dr \int_{-L_{\max}}^{L_{\max}} \frac{h(L) dL}{\sqrt{L_{\max}^2 - L^2}}. \quad (31)$$

In equilibrium, h is constant which means that one may write the integral in terms of the dimensionless variable $\tilde{L} = L/L_{\max}$ so that

$$dt \propto r dr \int_{-1}^{+1} \frac{d\tilde{L}}{\sqrt{1-\tilde{L}^2}}. \quad (32)$$

We thus find that in equilibrium the fraction of particles between r and $r+dr$ scales as $r dr$. Now at fixed a , the minimum and maximum radii attained by the particle are 0 and $2a$ so that the normalisation is such that

$$n_{eq}(r, a) = \frac{r dr}{2a^2} (r < 2a). \quad (33)$$

We can now find the surface density distribution by substituting $n(r, t, a) = n_{eq}(r, a)$ into Equations 28 and 29. Thus

$$\Sigma(r, t) \propto \frac{N(r, t)}{2\pi r} \propto \frac{1}{r} \int_{a_1}^{a_2} r a^{-5/2} da (a > r/2). \quad (34)$$

This gives rise to three regimes. For $0 < r < 2a_1$, all values of a contribute to the integral throughout this range and the surface density is *constant*. For $2a_1 < r < 2a_2$ then it is only a values greater than $r/2$ which contribute; consequently the surface density falls with radius as the annulus at r is populated by an ever decreasing range of a values. Finally, for $r > 2a_2$, no particles can be scattered to this radius and the surface density is zero.

Summarising we therefore have:

$$\Sigma(r) = A (0 < r < 2a_1), \quad (35)$$

$$\Sigma(r) = A \frac{(1 - (r/a_2)^{-3/2})}{1 - (a_1/a_2)^{-3/2}} (2a_1 < r < 2a_2), \quad (36)$$

$$\Sigma(r) = 0 (r > 2a_2). \quad (37)$$

We note that although we have derived the above for a specific distribution of particles in a , it is a *general* result that - in equilibrium - the surface density is uniform for radii less than twice the inner radius of the initial distribution. The reason for this is that every group of particles of given a is redistributed, in equilibrium, into a uniform density disc of particles extending from zero to $2a$. At every radial position inward of $2a_1$, *all* bins of a provide uniform surface density

contributions to the total surface density. It is only at radii $> 2a_1$ that particles with $a < r/2$ cease to contribute and the surface density starts to decline.

We emphasise that this entire derivation is based on the assumption that the disc fluctuations are scale-free, which implies that $\Delta\theta$ is independent of a and independent of phase at given a . In reality, however, the amplitude of perturbations in self-gravitating discs is an increasing function of radius. This changes the analysis in two ways: it changes the dependence of D on L (cf Equation 13) because the perturbations are of larger amplitude near apocentre and it also changes the scaling of D with a . As an example, if $(d\theta)^2 \propto r^p$ then the diffusion coefficient becomes (by analogy with Equation 12):

$$\langle D \rangle \propto a^p \int_{-e}^{+e} \frac{(GMa(1-x^2) - L^2)(1-x)^{p+1}}{\sqrt{(e^2 - x^2)}} dx. \quad (38)$$

In general, this integral is not analytic, except where $p=-1$: in this case the removal of the term $(1-x)$ makes no difference since the term $\propto x$ vanishes by symmetry for $p=0$. Consequently the evolution at fixed a still reduces to the Legendre equation, although the computation for a range of a now needs to take account of the additional a dependence of D . We do not pursue this further here, since - in considering situations that are likely to occur in real discs - we want to be able to treat cases other than $p=-1$. This forms part of our motivation for adopting a Monte Carlo method in the following section.

4.2 Monte Carlo simulations

We have checked and extended the above analysis of the behaviour of particle swarms that undergo diffusion in angular momentum at fixed energy by conducting simple Monte Carlo simulations. Here we subject co-planar particles (initially in circular orbits with the same surface density profile as employed in the SPH simulations) to random rotation of their velocity vectors through an angle in the range $\pm\Delta\theta$ at a random time each orbit. As expected, the evolution is qualitatively independent of the value of $\Delta\theta$ and with a timescale that scales as $\Delta\theta^{-2}$. We have adjusted our parameters so as to match the peak of the eccentricity distribution in the SPH calculation at a time $t = 5000$ and verified that the evolution of the eccentricity distribution (Figure 9) is in good agreement with the output of our analysis of the diffusion equation (Figure 8). Secondly, the early evolution compares reasonably well with the $f(e)$ curves obtained from the SPH simulation (Figure 4). However, the equilibrium distribution for $f(e)$ is only reached after several hundred thousand inner orbital periods.

We also looked at the evolution of the surface density distribution of the planetesimals with initial radii greater than $R=10$ (Figure 10), so as to compare with that for the SPH simulation (Figure 7). In the Monte Carlo simulation, the surface density profile evolves through a state similar to that seen in the SPH results and eventually attains a true equilibrium, where the surface density is approximately flat out to twice the inner radius ($R=20$) and declines to zero at twice the outer radius ($R=50$). This is the result expected from the earlier analysis.

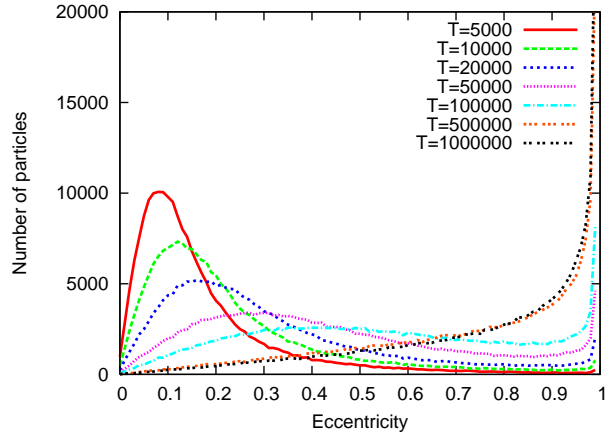


Figure 9. Evolution of the un-normalised eccentricity distribution from the Monte Carlo simulation.

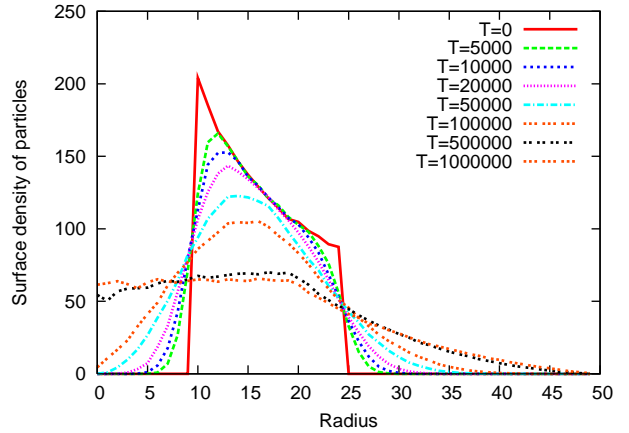


Figure 10. Evolution of the surface density distribution, in arbitrary units, from the Monte Carlo simulation.

4.3 Application to real discs

We have hitherto adopted the assumption that the fractional amplitude of perturbations - and hence the value of $\Delta\theta$ - is independent of radius. We have also normalised the evolution of the planetesimal swarm to that found in the SPH simulations which adopted rather short cooling times ($\beta = 5 - 10$) and correspondingly large amplitude of gravitational instability (with fractional amplitudes of several tens of percent (Cossins et al. 2010)). This choice was motivated by the need to compute the evolution of the planetesimal swarm in a reasonable time and also to ensure a sufficiently vigorous gravitational instability for it not to be quenched by numerical viscosity (Lodato & Clarke 2011). The insights provided by the simulations can now be used to rescale the problem to the parameter range expected in real self-gravitating discs.

We therefore consider the case of an optically thick self-gravitating disc accreting at $3 \times 10^{-6} M_{\odot} \text{ yr}^{-1}$ for which the steady state solutions (employing opacities due to dust and gas from Bell & Lin (1994)) are detailed in the Appendix of Clarke (2009). At radii > 35 au, the opacity is dominated by ice and we have:

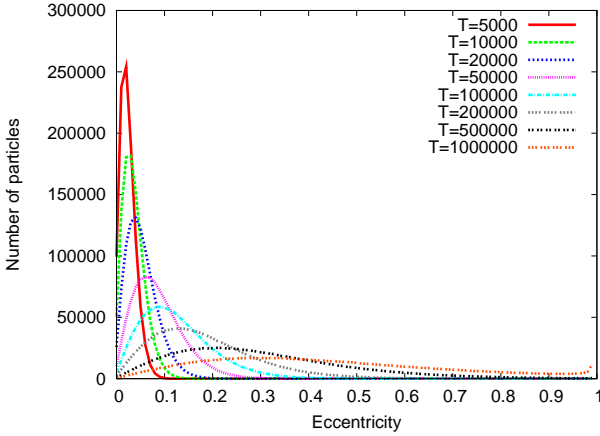


Figure 11. Evolution of the un-normalised eccentricity distribution from the Monte Carlo simulation with realistic cooling.

$$\beta = 3 \times 10^4 \left(\frac{R}{10 \text{ au}} \right)^{-9/2}. \quad (39)$$

For $22 \text{ au} < R < 35 \text{ au}$ (where opacity is dominated by ice sublimation) and

$$\beta = 270 \left(\frac{R}{10 \text{ au}} \right)^{-9/14}, \quad (40)$$

while for $4 \text{ au} < R < 22 \text{ au}$

$$\beta = 1000 \left(\frac{R}{10 \text{ au}} \right)^{-9/4}. \quad (41)$$

Since the amplitude of perturbations scales as $\beta^{-1/2}$ we also expect that $\Delta\theta \propto \beta^{-1/2}$; we normalise the value of $\Delta\theta$ at $\beta = 5$ in order to match the rate of evolution of the SPH simulation. Within $R = 4 \text{ au}$ we set $\Delta\theta = 0$ since it is arguable whether the disc is self-gravitating at this point; in any case, the long cooling times there equate to negligibly small values of $\Delta\theta$.

We start with a belt of planetesimals in circular orbits which are distributed with a power law surface density distribution with $\Sigma \propto R^{-3}$ since this is the steady state gas surface density profile for a self-gravitating disc with opacity dominated by ice grains (Clarke 2009). The belt extends from 60 to 100 au, the choice of inner radius being motivated by the fact that rather large amplitude density enhancements (rapid cooling) are required in order to form planetesimals through dust concentration in spiral arms (Clarke & Lodato 2009). A primary motivation for modeling a distribution with an initial hole is to discover whether - with a realistic prescription for the radial dependence of the perturbation amplitude - one expects planetesimals to be scattered inwards to fill up the hole over the self-gravitating lifetime of the disc.

We find (Figure 12) that the evolution is qualitatively similar to that in Figure 10: note that the edge is at 60 au in this simulation, as opposed to 10 code units in Figure 10. In both cases, the time is normalised to the dynamical time at the inner edge (1 code unit and 1 au respectively); therefore in order to compare the two plots at a given number of orbital times at the truncation point it is necessary to multiply the times in Figure 10 by $6^{1.5}$. It is then evident that the

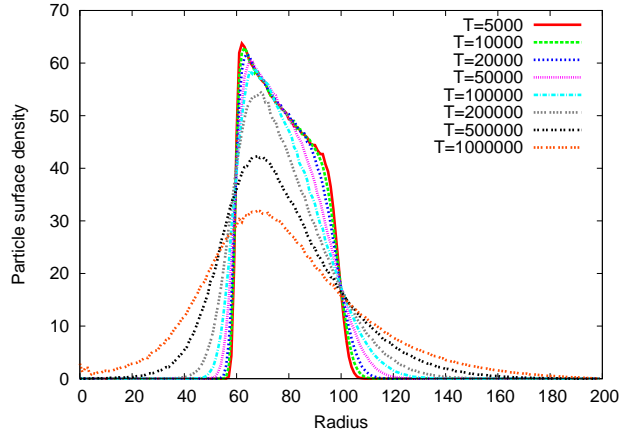


Figure 12. Evolution of the surface density distribution, in arbitrary units, from the Monte Carlo simulation with realistic cooling.

timescale for the infilling of the hole is rather similar in the two cases. i.e. the rate of infill is controlled by the amplitude of fluctuations near the truncation radius. This can be understood inasmuch that particles that visit the inner disc on eccentric orbits spend most of their time near apocentre (i.e. close to the truncation radius). The fact that - in the realistic variable β case - the spiral structure is of very low amplitude in the inner disc therefore has little effect on the evolution of the planetesimal swarm.

5 CONCLUSIONS

The SPH simulations indicate that planetesimal eccentricity is efficiently amplified by interaction with spiral features in self-gravitating discs. In the case of discs where the cooling time is not much longer than the dynamical timescale (i.e. in the outer disc, at radii > 10 s of au, where we expect planetesimals to be formed in such discs), the amplitude of these features is sufficient for high eccentricities (> 0.1) to be driven on much less than the self-gravitating lifetime of the disc. We have found that there is no significant velocity coherence within the particle swarm and thus that the local velocity dispersion is a significant fraction of the local orbital velocity; we also find that there is no tendency - in the test particle regime studied here - for the planetesimals to be concentrated within spiral arms. The lack of significant density enhancements and the large velocity dispersion (which weakens gravitational focusing) both contribute to very long collision times (> 1 Gyr); moreover, any collisions that did occur would be in the destructive regime.

We have used the SPH simulations to calibrate Monte Carlo experiments in which the particle direction is randomly perturbed around its orbit and have compared these Monte Carlo experiments with an analytical description. The Monte Carlo experiments allow the long time integration of the system and can also probe the high cooling time (weak spiral) regime that cannot be reliably simulated hydrodynamically. We have treated the case of an initial planetesimal belt at large radius (60 au) where the radial variation of the spiral amplitude is parametrised in terms of expected variations in the local cooling physics in marginally unstable self-gravitating discs. We find that - notwithstand-

ing the fact that the spiral potential is very weak at small radius - there is significant scattering of planetesimals into the inner disc, with particles that are perturbed in the region beyond 60 au visiting small radii on eccentric orbits. We nevertheless find that most of the particles initially beyond 60 au are likely to be retained at large radius on timescales of $\sim 10^5$ years.

The picture that emerges from this study is that if planetesimals do form in the self-gravitating phase of disc evolution then they will be retained in the disc throughout this phase; their high eccentricities inhibit collisions and mean that they will neither grow nor suffer significant collisional disruption over this period. If (as argued by Clarke & Lodato (2009)), such planetesimals are only formed in the outer disc then they will be largely retained at such radii, though with a significant minority that are perturbed to the inner regions of the disc. Such an endpoint would therefore represent the initial conditions for considering the subsequent evolution of planetesimals during the non-self gravitating phase of disc evolution.

ACKNOWLEDGEMENTS

JJW thanks the STFC for his studentship. We would like to thank Guiseppe Lodato for providing much valuable advice, Mark Wyatt and Jim Pringle for discussion and comments, and John Eldridge for proof-reading the paper.

REFERENCES

- Adachi I., Hayashi C., Nakazawa K., 1976, *Progress of Theoretical Physics*, 56, 1756
 Adams F. C., Bloch A. M., 2009, *ApJ*, 701, 1381
 Bate M. R., Bonnell I. A., Price N. M., 1995, *MNRAS*, 277, 362
 Bate M. R., Lubow S. H., Ogilvie G. I., Miller K. A., 2003, *MNRAS*, 341, 213
 Bell K. R., Lin D. N. C., 1994, *ApJ*, 427, 987
 Benz W., Asphaug E., 1999, *Icarus*, 142, 5
 Binney J., Tremaine S., 2008, *Galactic Dynamics: Second Edition*. Princeton University Press
 Boss A. P., 2000, *ApJ*, 536, L101
 Britsch M., Clarke C. J., Lodato G., 2008, *MNRAS*, 385, 1067
 Clarke C. J., 2009, *MNRAS*, 396, 1066
 Clarke C. J., Lodato G., 2009, *MNRAS*, 398, L6
 Cossins P., Lodato G., Clarke C., 2010, *MNRAS*, 401, 2587
 Cossins P., Lodato G., Clarke C. J., 2009, *MNRAS*, 393, 1157
 Gammie C. F., 2001, *ApJ*, 553, 174
 Gibbons P. G., Rice W. K. M., Mamatsashvili G. R., 2012, *MNRAS*, 426, 1444
 Greaves J. S., Richards A. M. S., Rice W. K. M., Muxlow T. W. B., 2008, *MNRAS*, 391, L74
 Hubickyj O., Bodenheimer P., Lissauer J. J., 2005, *Icarus*, 179, 415
 Ida S., Guillot T., Morbidelli A., 2008, *ApJ*, 686, 1292
 Kokubo E., Ida S., 2000, *Icarus*, 143, 15
 Laughlin G., Bodenheimer P., Adams F. C., 2004, *ApJ*, 612, L73

- Leinhardt Z. M., Stewart S. T., Schultz P. H., 2008, *Physical Effects of Collisions in the Kuiper Belt*, Barucci, M. A., Boehnhardt, H., Cruikshank, D. P., Morbidelli, A., & Dotson, R., ed., pp. 195–211
 Lodato G., Clarke C. J., 2011, *MNRAS*, 413, 2735
 Lodato G., Rice W. K. M., 2005, *MNRAS*, 358, 1489
 Meru F., Bate M. R., 2011, *MNRAS*, 410, 559
 —, 2012, *ArXiv e-print:1209.1107*
 Nelson R. P., 2005, *A&A*, 443, 1067
 Nelson R. P., Gressel O., 2010, *MNRAS*, 409, 639
 Nelson R. P., Papaloizou J. C. B., 2004, *MNRAS*, 350, 849
 Paardekooper S.-J., 2012, *MNRAS*, 421, 3286
 Paardekooper S.-J., Baruteau C., Meru F., 2011, *MNRAS*, 416, L65
 Pollack J. B., Hubickyj O., Bodenheimer P., Lissauer J. J., Podolak M., Greenzweig Y., 1996, *Icarus*, 124, 62
 Rice W. K. M., Forgan D. H., Armitage P. J., 2012, *MNRAS*, 420, 1640
 Rice W. K. M., Lodato G., Pringle J. E., Armitage P. J., Bonnell I. A., 2004, *MNRAS*, 355, 543
 —, 2006, *MNRAS*, 372, L9
 Safronov V. S., 1969, *Evolutsiia doplanetnogo oblaka*.
 Stamatellos D., Whitworth A. P., Bisbas T., Goodwin S., 2007, *A&A*, 475, 37
 Takeuchi T., Clarke C. J., Lin D. N. C., 2005, *ApJ*, 627, 286
 Tanaka H., Ward W. R., 2004, *ApJ*, 602, 388
 Toomre A., 1964, *ApJ*, 139, 1217
 Wyatt M. C., Smith R., Greaves J. S., Beichman C. A., Bryden G., Lisse C. M., 2007, *ApJ*, 658, 569

APPENDIX A: INTEGRATING AROUND AN ORBIT

The expected value of D is obtained by averaging over one orbit. This requires obtaining dt as a function of r . We start with the orbital equation for r as a function of ϕ .

$$r = \frac{a(1 - e^2)}{1 + e \cos \phi} \quad (\text{A1})$$

$$\frac{dr}{dt} = \frac{dr}{d\phi} \frac{d\phi}{dt} = \frac{dr}{d\phi} \frac{L}{r^2} \quad (\text{A2})$$

L is a constant of the motion for given values of a and e .

$$L^2 = GMa(1 - e^2) \quad (\text{A3})$$

$$\frac{dr}{dt} = \frac{a(1 - e^2)e \sin \phi}{(1 + e \cos \phi)^2} \frac{\sqrt{GMa(1 - e^2)}}{r^2} \quad (\text{A4})$$

Substituting r back in simplifies the expression.

$$\frac{dr}{dt} = \frac{\sqrt{GMa} \sin \phi}{1 - e^2} \frac{1}{a} \quad (\text{A5})$$

Re-arranging Equation A1 and using that to eliminate ϕ gives an expression in r and e only.

$$\frac{dr}{dt} = \frac{\sqrt{GMa}}{r} \sqrt{e^2 - (1 - r/a)^2} \quad (\text{A6})$$